PCCP

ROYAL SOCIETY OF CHEMISTRY

PAPER

View Article Online
View Journal | View Issue

Check for updates

Cite this: *Phys. Chem. Chem. Phys.*, 2022, **24**, 23849

A wear-resistant silicon nano-spherical AFM probe for robust nanotribological studies†

Paul C. Uzoma,[a] Xiaolei Ding,[a] Xiaolei Wen,[c] Lansheng Zhang,[a] Oleksiy V. Penkov*[ad] and Huan Hu*[abd]

Nanoscale wear can severely limit the performance of tips used in atomic force microscopy, especially in contact and lateral mode operations. Hence, we investigated the mechanical and tribological properties of a newly invented nano-spherical silicon tip produced *via* swelling of single-crystal silicon using helium ion dosing to ascertain its reliability for AFM operations. The nanoindentation test proved that the modulus of elasticity of the nano-spheres tends to increase with the diameter of the spheres at 0.5 mN contact force. However, at 10 mN higher contact force, the elastic modulus was stable at ~160 GPa irrespective of the sphere diameter. The SEM images confirmed the durability of the tip after 10 000 cycles of sliding on a silicon wafer and quartz surfaces. There was no damage on the tip and the wear debris was suggested to be from the localized wear on the counter wafer surface. Also, the *in situ* AFM pull-off force test indicated that the geometry of the tip remained unaltered during the wear test. The Si/SiO_2 tribology study showed a decrease in coefficient of friction as velocity and sliding cycles increased which was attributed to the tribochemical reactions occurring at the Si/SiO_2 interfaces. These results indicate that the new nano-spherical AFM tip has advantages in nanoscale tribology measurement.

Received 11th July 2022,
Accepted 13th September 2022

DOI: 10.1039/d2cp03150g

rsc.li/pccp

Published on 13 September 2022. Downloaded by Zhejiang University on 2/23/2024 3:47:54 AM.

1. Introduction

Atomic force microscopy (AFM) is considered a vital instrument in nanotechnology with constantly increasing application potential in electronics,[1,2] tribology,[3,4] cell and molecular biology,[5,6] materials designs,[7,8] polymers,[9,10] energy storage and generation,[11,12] *etc.* In AFM operation, an AFM probe raster scans over a sample, and the identified tip-sample interaction force shows the morphology and other physical properties at nanoscale resolutions.[13] The properties of the probe including the tip significantly influence the measurement resolution, sample integrity, reliability, *etc.*

Colloidal AFM tips[14] otherwise known as spherical AFM tips have shown interesting applications including the measurement of biological force, colloidal force, adhesive force mapping, interactions of particles relative to pharmaceutical aerosols, nanomanipulation, and nanolithography.[15–18] Generally, the spherical probe is known as a non-destructive approach to measuring surface properties. Interestingly, the advancement in the use of AFM techniques from laboratory research to industrial applications has made the performance and stability of AFM tips paramount. This is because several studies have shown that the deformation and wear of AFM tips place a serious limitation on their performance.[19–22] An ideal tip should be chemically stable and exhibit good wear and contamination resistance for a prolonged period of usage.

Silicon (Si) is one of the most common materials used in AFM probe fabrication, but its moderate mechanical properties have made silicon tips susceptible to failure through the brittle fracture mechanism. Also, their natural hydrophilic oxidized surfaces with high adhesion make them prone to accelerated environmental degradation.[23,24] Over the decades, the study of the tribological properties of silica surfaces has received huge attention because of its technological application potential such as wafer planarization for the production of micro/nano-electromechanical systems (MEMS/NEMS) and wafer bonding in nanoengineering of semiconductors.[25,26] There is also the tribology of silica surfaces in geophysics and earthquake mechanisms because silica is a common constituent of rocks, and frictional instabilities in crustal faults are known to result in shallow tectonic earthquakes.[27,28]

[a] *ZJU-UIUC Institute, International Campus, Zhejiang University, Haining, 314400, China. E-mail: oleksiypenkov@intl.zju.edu.cn, huanhu@intl.zju.edu.cn*
[b] *State Key laboratory of Fluidic Power & Mechatronic Systems, Zhejiang University, Hangzhou, China*
[c] *Center for Micro and Nanoscale Research and Fabrication, University of Science and Technology of China, Hefei, 230026, China*
[d] *Department of Mechanical Science and Engineering, University of Illinois at Urbana-Champaign, Urbana, IL, 61801, USA*

† Electronic supplementary information (ESI) available. See DOI: https://doi.org/10.1039/d2cp03150g

Published on 13 September 2022. Downloaded by Zhejiang University on 2/23/2024 3:47:54 AM.

This work discusses the tribology of the Si/SiO_2 interface by sliding our newly invented Si nano-spherical tip against SiO_2 surfaces. The Si/SiO_2 interface is a dominant feature in MEMS/NEMS, and since these systems are very small with tight clearance, their overall output strongly depends on the Si/SiO_2 tribology. Silica surfaces have been reported to form strong Si–O–Si links across the interface *via* the dehydroxylation reaction between two hydroxyls from each silica surface.[29] These strong covalent Si–O–Si bridges pull atoms out of the surface of the silica or break during frictional sliding leading to localized surface wear. Li *et al.*[29] employed molecular dynamics to study the static friction behavior between amorphous silica surfaces with varying interfacial siloxane (Si–O–Si) bridges. They reported a nonlinear increase in the static friction force with the concentration of interfacial siloxane bridges, which was attributed to the interactions among neighboring bridges. They also explained the atomic scale wear mechanisms of silica to be due to the transfer of individual atoms followed by breaking interfacial siloxane bridges and transfer of atomic clusters initialized by rupturing of surface Si–O bonds. Also, continuous formation and dissolution of small clusters at the sliding interface were found to play a significant part in wear at the silica/silica interface. Yeon *et al.*[30] *via* ReaxFF-MD simulations confirmed that a large number of atoms are transferred across the silica interface during the sliding. The existence of submonolayer thick H_2O was shown to lend additional reaction pathways to form the Si–O–Si bridges and transfer of atoms across the interface. But full monolayer thick H_2O can significantly reduce the rate of atom transfer because the silicon atoms at the sliding interface can no longer form Si–O–Si bridges since they are terminated with hydroxyl groups. Interestingly, reports have shown that the chemical reactions occurring at silica/silica sliding contacts can result in contact aging which is described as an increase in the static friction as a function of time during which the surfaces are held in contact prior to sliding.[31] Chen *et al.*[32] used AFM and TEM techniques to investigate the wear of the Si/SiO_2 sliding interface. Under humid conditions, they showed that there is no mechanically influenced subsurface damage in the wear track, which is in agreement with the assumption that wear under humid conditions is strictly tribochemical. The tribochemical reactions were shown to take two directions. First is the dehydration reaction between silanol groups at the surfaces resulting in wear, and second is the dehydration reaction between adjacent silanol groups on one solid surface leading to a low-friction state.

Previously, our group reported a new approach to fabricating nano-spherical AFM tips *via* the use of high-energy helium ion dosing.[33] See Fig. S1 in the ESI† which shows the SEM image of the nano-spherical tip. Ref. 33 proved accurate control of the amorphous silicon nano-spheres (100 nm to 1 μm diameter range) by regulating the helium ion dose from 10 000 ions nm^{-2} to 40 000 ions nm^{-2}. Also, the precise placement of spheres with 10 nm lateral resolution was reported. The new tip can obtain clear images in both AC and contact mode operations.[33] To further examine the reliability and the advantages of the new nano-spherical tip for tribology purposes, this current work used a UNHT^3 ultra-high-resolution nanoindenter, an AFM, and a scanning electron microscope (SEM) to evaluate the mechanical and tribological properties of the nano-spherical tip, particularly when sliding against a quartz substrate. It is interesting to note that the use of an AFM to study wear and friction at the nanoscale can give valuable insights into the principle wear mechanisms leading to an improved understanding of the key factors of failure from big machines to micromachines.[34,35]

2. Experimental

A UNHT^3 (Anton Paar) nanoindenter was used to measure the mechanical properties of the silicon nano-sphere, silicon wafer, and quartz samples. The spherical-shaped indenter was used for the nano-sphere while the pyramidal indenter was used for the wafer and quartz samples. The indenter was pressed into the surface of the silicon nano-sphere while monitoring the depth and normal load. The mechanical properties were obtained from the force-displacement curve according to the ISO 14577 standard.

Furthermore, two different surfaces were used to determine the wear resistance of the nano-spherical and sharp AFM tips; polished silicon wafer and quartz with 0.227 nm and 0.701 nm roughness, respectively. The silicon wafer and the quartz samples were ultrasonically cleaned in acetone, propanol, ethanol, and distilled water respectively before drying with nitrogen gas. The tribology test was done using an Asylum MFP-3D AFM. All the tests were carried out in air at 24 °C temperature and ~38% relative humidity. Before each test, the stiffness of the cantilevers was measured using the thermal method, which depends on the equipartition theorem from classical thermodynamics relating the mechanical fluctuations of the cantilever with its thermal energy.[36] The radius, spring constant, and resonance frequency of the nano-spherical tip are ~185 nm, ~2.4 N m^{-1}, and ~70 kHz, respectively. Also, the radius, spring constant, and resonance frequency of the commercial sharp tip (Fig. S2, ESI†) are 7 nm, ~2 N m^{-1}, and ~70 kHz, respectively. 10 000 friction cycles were performed during the wear tests corresponding to the 0.2 m scan distance on a 20 μm × 20 μm surface area. Unless stated otherwise, the applied normal load is ~240 nN at a 1 Hz loading rate and a 10 μm s^{-1} sliding speed. The progress of the tip degradation was monitored *in situ* by measuring the tip-substrate pull-off adhesion force every 1000 cycles.

The scanning electron microscope (GeminiSEM 300) was used to observe the different samples and monitor the extent of tip degradation after the wear test. The water droplet imaging system and the ImageJ software were used to measure the water contact angle of the droplets on the quartz sample.

3. Results and discussion

3.1 Nanoindentation test

An array of silicon nano-spheres was fabricated by helium ion implantation on a silicon wafer (Fig.(1a)) and the nanoindentation

 This journal is © the Owner Societies 2022

Published on 13 September 2022. Downloaded by Zhejiang University on 2/23/2024 3:47:54 AM.

test was carried out as shown in Fig. 1(b). The SEM images of the different sizes of the nano-spheres are also shown in Fig. S3 (ESI†). At 0.5 mN maximum contact force and 0.2 mN min^{-1} loading and unloading rate, the test proves that the elastic modulus of the nano-spheres increases with the diameter (Fig. 1(c)) indicating that a higher degree of helium ion dose increases the resistance to elastic deformation at very low loads. *Via* atomistic calculations and experimental measures, researchers have demonstrated that elastic behavior is dependent on the size at the nanoscale; as the dimensions approach the nanoscale, the higher the elastic property deviation from bulk values.[37–39] This observation was attributed to the surface effects which include surface elasticity and surface oxidation.[40,41] Since the diameters of the nanospheres are $\geq$200 nm, the surface effect can be neglected. Therefore, the observed increase in the indentation modulus can be ascribed to the increase in helium ion doses which has modified the internal structures, density, and wall thickness of the nanospheres as seen in ref. 33. It is worth noting that several reports have proved that the mechanical properties of silicon can be modified by the implantation of appropriate ion species and doses.[42–44] The plot further shows that the resistance to plastic deformation was not significantly affected by the increase in the diameter. The force–displacement curve (Fig. 1(d)) gives a maximum penetration depth of ~20 nm for all the nanospheres and showed no obvious discontinuity suggesting any evidence of crack propagation during the indentation processes. Meanwhile, at a higher contact force of 10 mN and 0.2 mN min^{-1} loading/unloading rate, the penetration depth is higher in the 800 diameter sphere (145 nm) whereas the other spheres maintained ~130 nm penetration depth as shown in Fig. S4 (ESI†). The elastic modulus and resistance to permanent deformation remained stable at ~160.6 GPa and ~9.84 Gpa for all the samples. This difference in elastic modulus due to the change of load during nanoindentation has been referred to as the load effect which can be attributed to different developments such as indentation elastic recovery, plastic deformation band spacing, work hardening during indentation, *etc.*[45] Although some works have shown that strain rates can significantly affect the deformation of nanoparticles,[46,47] in our case, the same strain rate was used during the experiment. There is no observable evidence of crack propagation as seen in Fig. S4 and S5 (ESI†) (SEM images after the nanoindentation test). Furthermore, since our nano-spheres are bubble-like (hollow), they can withstand longer strain to deformation than solid spheres obtained through other design techniques as confirmed in the literature; while solid nanoparticles can have great strength at the expense of deformation, hollow silicon nanoparticles are known to maintain strength and ductility.[48,49]

3.2 AFM wear resistance test

Fig. 2 shows the SEM images of the nano-spherical tip after the wear test. The tip is largely unaffected after the test and neither

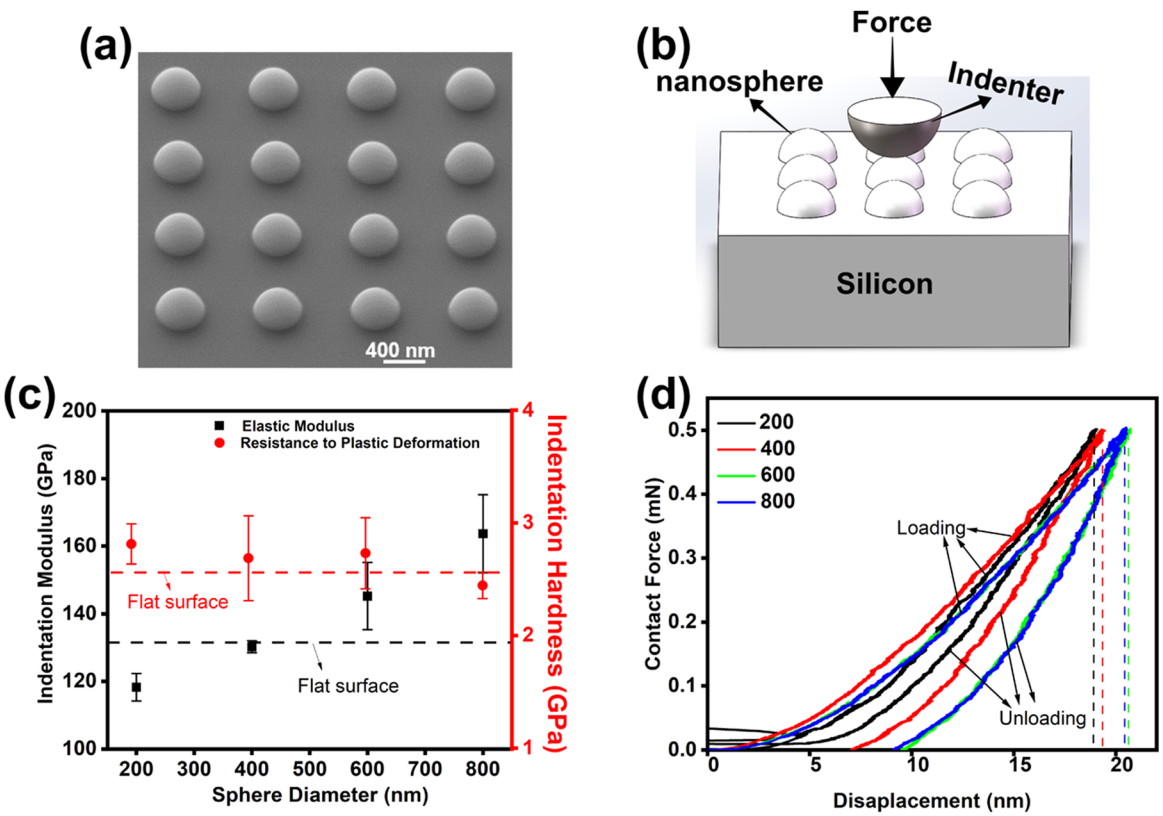

Fig. 1 (a) SEM image of 400 nm diameter spherical nano-spheres. (b) Schematic representation of the nanoindentation test using the spherical indenter. (c) Plot of elastic modulus and resistance to plastic deformation against the sphere diameter at 0.5 mN force. (d) Plot of contact force against displacement for the different nanopsheres (200 nm, 400 nm, 600 nm, and 800 nm diameters).

Published on 13 September 2022. Downloaded by Zhejiang University on 2/23/2024 3:47:54 AM.

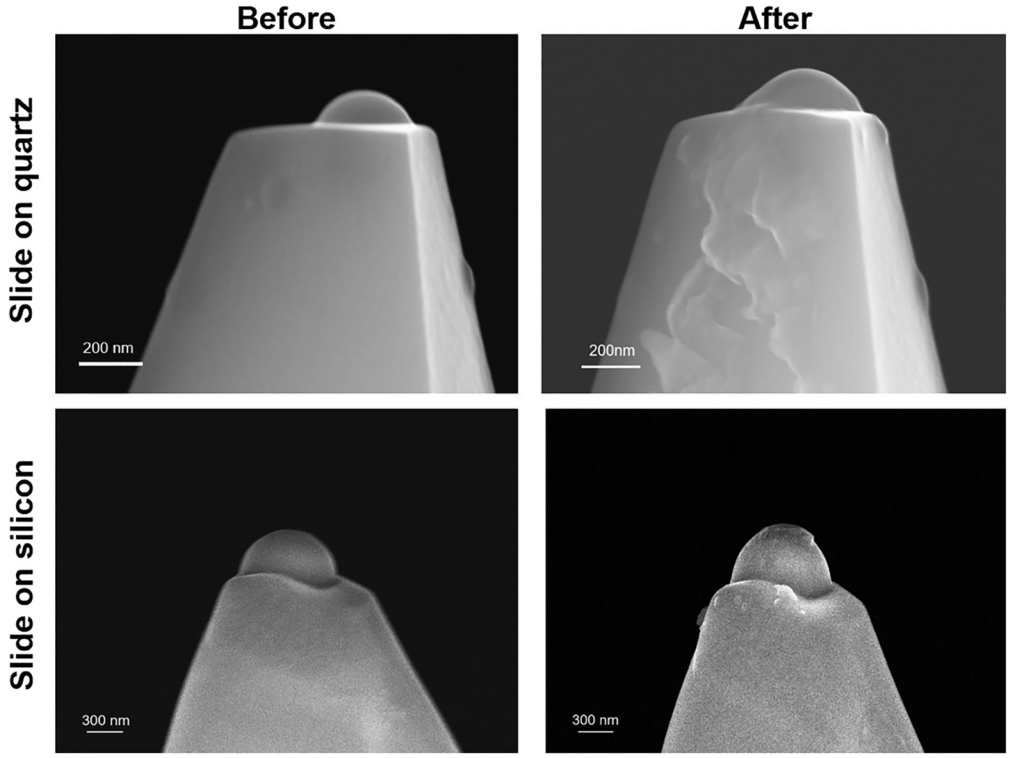

Fig. 2 SEM images of the nano-spherical tips before and after the wear test.

deformation nor delamination is observed indicating the remarkable durability. Fig. S6 (ESI†) shows the presence of wear debris on the tip used to slide on the wafer's sample. The wear debris is suggested to come from the localized surface wear on the wafer's surface resulting from the breaking of the Si–O–Si bridges as previously mentioned. Meanwhile, there is no observable wear debris on the tip used on the quartz sample.

In contrast, sliding the sharp tip against the silicon and quartz samples destroyed the sharp tip as shown in Fig. 3. Also, there is a large accumulation of wear debris on the tip after the wear test, especially on the tip sliding on the quartz surface. The AFM image of the quartz sample after a few sliding cycles shows increased roughness, another indication of wear at the sliding interfaces (Fig. S7, ESI†). Besides tip wear, tip fouling is considered the most common factor responsible for probe failure in normal AFM operations and it can significantly reduce the tip performance.[50]

Pull-off forces of the nano-spherical and commercial sharp tips on the quartz sample were measured every 1000 cycles. The Derjaguin–Muller–Toporov (DMT) model of contact mechanics can be used to evaluate the pull-off interactions between the silicon tips and the quartz sample.[51] The DMT model proves that even though the van der Waals' forces can increase the elastic contact area between the ball and the plane, the force needed to overcome the molecular forces arising when the contact is broken does not increase thereby. This model is generally applied to weak, long-range adhesion between stiff materials. Herein, the interaction between the AFM tip and the sample is modeled as a sphere in contact with a flat plane as shown in Fig. 4(a), it expressed the pull-off force (F_p) as shown in eqn (1) where "W" is the work of adhesion and "R" is the tip radius.

$$F_p = 2\pi WR \quad (1)$$

The measurement of the pull-off force gives an indirect approach for recording the changes in tip geometry during the wear test.[52,53] The plot in Fig. 4(b) shows no significant change in the values of the pull-off forces for the nano-spherical tip throughout the sliding period. The distant point observed at 2000 and 8000 cycles might be due to localized contamination as described elsewhere.[53] Also, employing eqn (1), the work of adhesion before and after sliding the nano-spherical tip on the quartz sample are 98.1 mJ m^{-2} and 95.5 mJ m^{-2} respectively which indicates a relatively constant work of adhesion, hence, confirming that there is no obvious change in the tip geometry. In contrast to the spherical tip, the sharp tip shows an increase in the pull-off force which is consistent with the significant changes observed in the SEM images. In addition, the work of adhesion before and after sliding on the quartz substrate is 495 mJ m^{-2} and 28 mJ m^{-2} respectively which confirms a significant change in the tip's geometry.

The importance of the AFM tip's wear-resistant properties particularly in nanotribology is further understood from Fig. 5, which shows the height profile of the quartz sample obtained using the sharp and nano-spherical tips during the wear tests. The plot was taken from the topographic AFM images 1–4 representing a scan distance of 10–40 mm. It is good to note that the AFM image exhibits a convolution of both the real

 This journal is © the Owner Societies 2022

Published on 13 September 2022. Downloaded by Zhejiang University on 2/23/2024 3:47:54 AM.

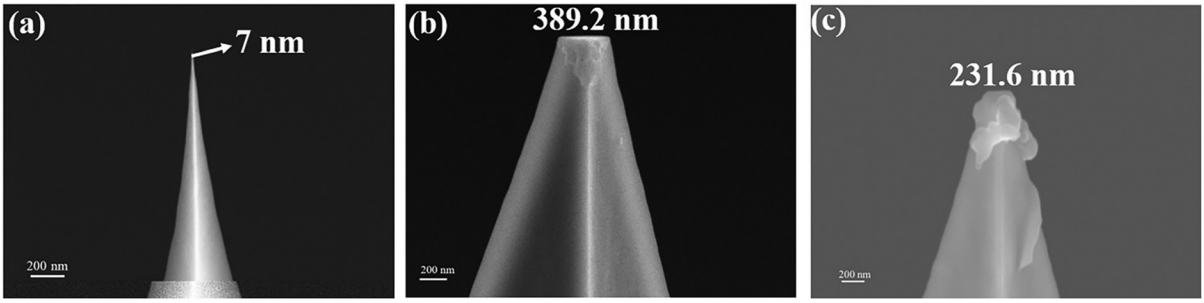

Fig. 3 SEM images of the commercial sharp tips at 200 nm scale. (a) Before the wear test, the tip's diameter is 7 nm, (b) after sliding on the wafer's surface, the tip suffered significant damage and the sharp point was degraded. (c) After sliding on the quartz sample, the sharp point was degraded and there is a high accumulation of wear debris. The applied normal load during the AFM test is ~240 nN.

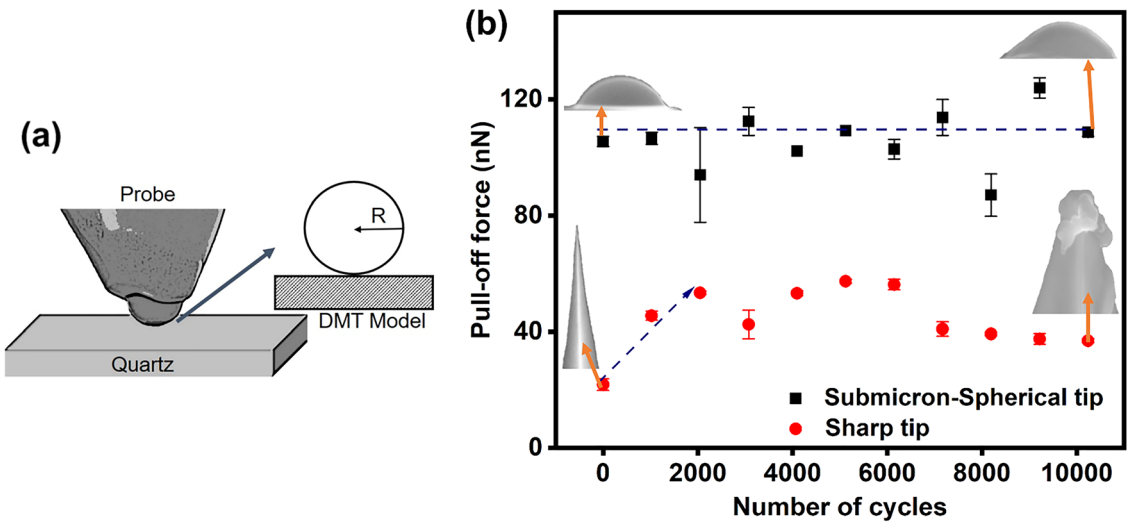

Fig. 4 (a) Schematic of the DMT model describing the interaction between the tip and the quartz sample. (b) Pull-off forces of the nano-spherical and commercial sharp tips on the quartz sample as a function of sliding cycles. The insets show the SEM images of the tips before and after the sliding at 200 nm scale.

features of the sample and the geometry of the scanning tip.[54] The nano-spherical tip exhibited a steady and constant height profile whereas the sharp tip showed a great degree of variation in the height profile of the quartz sample. This high degree of variation can be attributed to tip damage and localized fouling arising from the detachment and attachment of nanoscale wear debris as seen in Fig. 3(c). Practically, the new nano-spherical probe is well suited for contact mode AFM operation since it is ultra-smooth (~0.1 nm roughness)[55] and does not wear easily, whereas it is very difficult to complete a contact mode full scan using the sharp probe (without replacement) because it can easily wear off.

To further explore the tribology of Si/SiO_2 experienced during the sliding of the nano-spherical tip against the quartz sample, contact radius (α) and pressure (P) achieved during sliding were calculated using the DMT model as expressed in eqn (2)–(4):

$$a = \left(\frac{FR}{K}\right)^{\frac{1}{3}} \quad (2)$$

where F is the total load acting on the tip which includes the normal force (240 nN) and the adhesion force (106 nN). K (68.13 GPa) is the composite modulus of elasticity obtained using eqn (3).

$$k = \frac{4}{3}\left(\frac{1-\nu_1^2}{E_1} + \frac{1-\nu_2^2}{E_2}\right)^{-1} \quad (3)$$

where ν_1 and ν_2 are the Poisson ratios of the tip and quartz sample respectively, and E_1 (160 GPa) and E_2 (70 GPa) are the elastic moduli of the silicon and quartz, respectively. The average contact pressure P_{avg} is obtained by dividing the total load by the contact area:

$$P_{avg} = \frac{F}{\pi a^2} \quad (4)$$

The contact radius (α) is 9.54 nm and the peak normal contact pressure P_{max} (P_{max} = 1.5 P_{avg}) is 5.7 GPa which is lower than the hardness values of the Si (6.5 GPa) and SiO_2 (7.0 GPa) (these hardness values were obtained using the pyramid-shaped nanoindenter). The indentation deformation is expected to mostly

Published on 13 September 2022. Downloaded by Zhejiang University on 2/23/2024 3:47:54 AM.

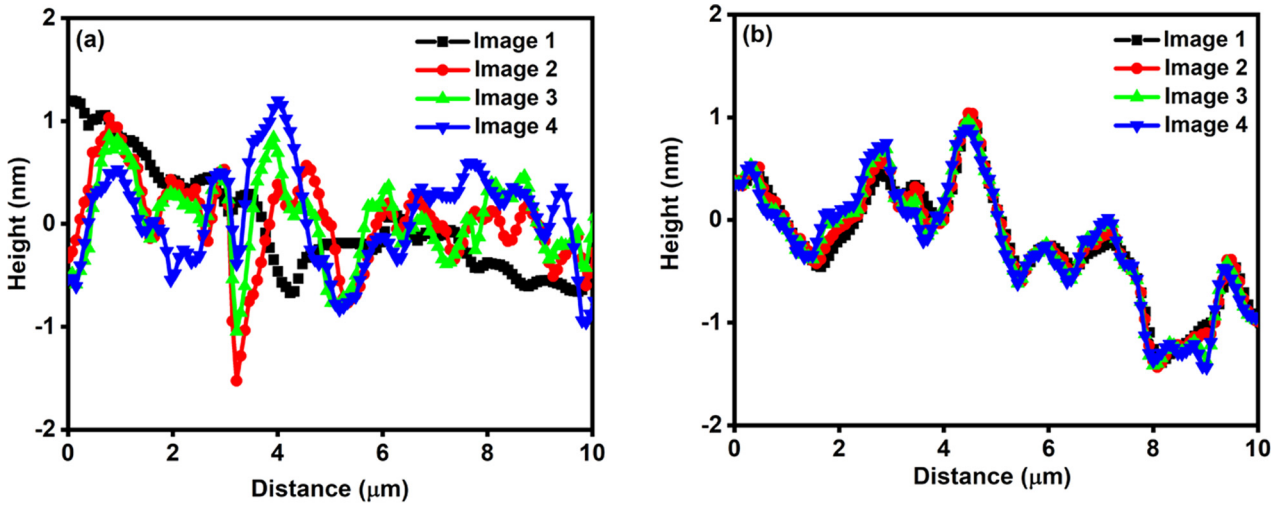

Fig. 5 Height profile obtained from AFM images at the initial stages of sliding (a) commercial sharp (b) nano-spherical tip on quartz samples. The applied normal load during the AFM test is ~240 nN.

occur on the quartz sample with a lower elastic modulus which agrees with the fact shown in the SEM image (Fig. 1) that neither deformation nor delamination was observed on the spherical probe.

3.3 Si/SiO_2 friction analysis

Fig. 6 shows the friction measurement of the nano-spherical probe on the quartz sample. The coefficient of friction was found to decrease with an increase in velocity and number of sliding. Decreasing friction with increasing velocity is reported when silica surfaces are terminated with a hydroxyl group (–OH).[29,30] This is because –OH groups can form hydrogen bond networks at the interface and low sliding velocity results in the formation of a more extensive stronger hydrogen bond network.[56] Contrary to bulk silica, silica surfaces are susceptible to linking with chemical groups since they have significantly lost the complete tetrahedral configuration.[57] This enables the –OH group to link with silicon atoms on silica surfaces through Si–O covalent linkages. A higher concentration of the –OH groups will impact the hydrophilic behavior on the silica surface resulting in the absorption of water molecules *via* the formation of H-bonds with the surface hydroxyls.[29] Interestingly, the water contact angle of the quartz sample is 35° confirming the hydrophilic behavior (Fig. S8, ESI†). Besides the hydrogen bond network, covalent bonding through interfacial siloxane bridges, colloidal interactions, and capillary force of a condensed H_2O meniscus are other silica surface interactions that play a key role in the tribology of Si/SiO_2.[58–61]

Furthermore, the coefficient of friction was shown to decrease sharply at the initial stages of sliding and slowed as sliding continues (see also Fig. S9, ESI†) similar to what is obtained in the macroscale experiment. However, at the macroscale, the reduction in friction during the initial stages of sliding (running-in process) is generally associated with the decrease in the contact pressure after rough asperities on the contact interface are smoothened under mechanical action.[62] This asperity flattening mechanism cannot describe the decrease in friction experienced in the sliding of the silicon

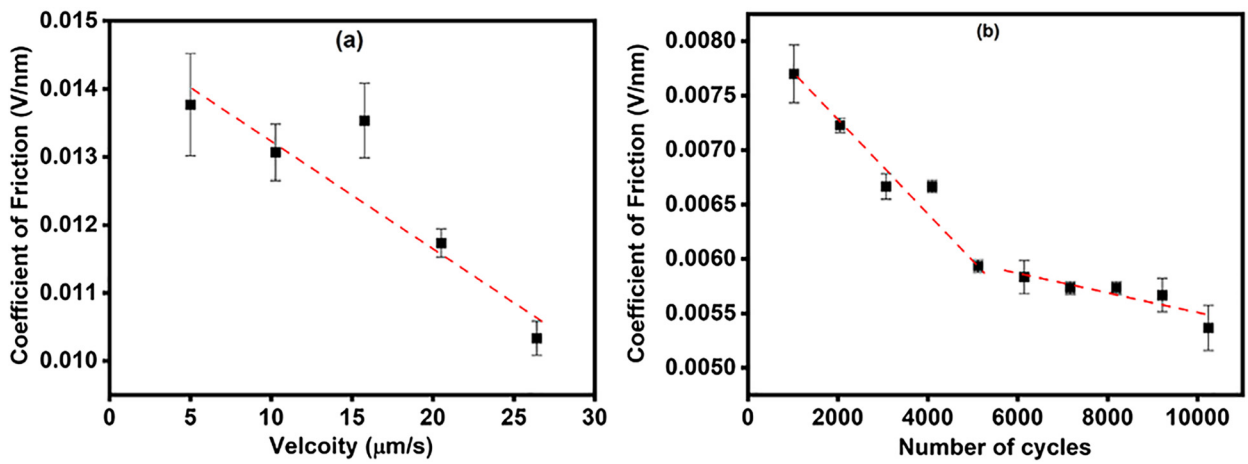

Fig. 6 Plots of coefficient of friction against (a) velocity and (b) sliding cycles using the nano-spherical tip.

 This journal is © the Owner Societies 2022

Published on 13 September 2022. Downloaded by Zhejiang University on 2/23/2024 3:47:54 AM.

nano-spherical tip against the quartz sample since their interface gave a single asperity contact during the test. Since the classical Amonton's law cannot be used to describe the friction force at the nanoscale, the model proposed by Tambe *et al.*[63] can be employed to analyze the Si/SiO_2 nanoscale friction. Tambe *et al.* suggested that the nanoscale friction between contact interfaces is due to three components as expressed in eqn (5).

$$F_t = F_{int} + F_{def} + F_{stick\text{-}slip} \quad (5)$$

where F_{int} is the friction force due to the interfacial adhesion between the Si/SiO_2, F_{def} friction force due to the deformation at the interfaces of Si/SiO_2, and $F_{stick\text{-}slip}$ friction force due to stick-slip between the Si/SiO_2 contact interfaces. At the atomic scale, stick-slip amounts to the energy needed for the tip to jump from a steady equilibrium position on the quartz's surface into a neighboring position.[63] There is no effect of $F_{stick\text{-}slip}$ because a frictional process without stick-slip was observed during the experiment. Also, Fig. 3 shows an insignificant change in the Si/SiO_2 interfacial adhesion throughout the sliding cycle thereby limiting the contribution of F_{int}. The F_{def} is calculated as the sum of the plastic deformation-related friction force ($F_{def\text{-}p}$) and the elastic deformation-related friction force ($F_{def\text{-}e}$).[64] Because the deformation is not completely due to mechanical shearing, $F_{def\text{-}p}$ will not be considered. Eqn (6) gives the relationship between the $F_{def\text{-}e}$, the total load (F), the radius of the probe (R), and the contact radius (α).[65]

$$F_{def\text{-}e} = \frac{2F}{\pi a^2}\left(R^2 \sin^{-1}(a/R) - a\sqrt{R^2 - a^2}\right) \quad (6)$$

The value of F is considered to be fairly stable throughout and there is a very slight change in R indicating that the contribution of $F_{def\text{-}e}$ to the decrease in friction is also minimal. This is in agreement with Tambe *et al.*[63] who stated that even though there is the presence of adhesion and interfacial interactions during sliding, the extent of their influence on friction can be limited by several factors. Therefore, the decrease in friction can be largely due to the chemical reaction induced by the mechanical shearing. It is suggested that the mechanical shear could affect the Morse potential of specific chemical bonds at the interface thereby reducing the energy barrier for bond breakage.[66] The absence of wear debris on the spherical probe, and the stable height profile of the quartz sample shown in Fig. 5(b) confirm that tribochemical wear instead of mechanical wear is the major reason for the decrease in friction. Besides, Chen *et al.* proved that the tribochemical reaction dominates nanoscale friction of Si/SiO_2, and the dehydration reactions between adjacent silanol groups on one solid surface can result in a low-friction state.[32,64] Similar results have been reported elsewhere.[67,68]

4. Conclusion

The durability of a silicon nano-spherical AFM tip fabricated *via* higher-energy helium ion dosing has been confirmed. At 0.5 mN low contact force, the modulus of elasticity was found to increase with the increasing nano-sphere diameter while the plastic deformation value remains unchanged. Besides, the mechanical properties remained stable irrespective of the diameter of the nano-spheres at a higher load (10 mN). These improved mechanical properties are attributed to the bubble-like and ultra-smooth nature of the nano-spheres and the ion doses which modified the internal structure, density, and wall thickness of the nano-spheres. The friction and wear analysis at ~240 nN normal load showed that the tip geometry remained almost unchanged after 10 000 cycles of sliding confirming the reliability of the tip for AFM contact and lateral mode operations. Also, the associated wear and friction mechanism was found to be a function of tribochemical reaction at the sliding interfaces; an interesting factor to consider in practical applications of the tip and for Si/SiO_2 interface designs.

Author contributions

H. Hu and O. Penkov created the concept and designed the experiment. P. Uzoma performed the tribology test, analyzed the data, and drafted the manuscript. X. Ding performed the SEM test. X. Wen performed the helium ion implantation test and L. Zhang did the wettability test. H. Hu and O. P reviewed the paper and provided revisions.

Conflicts of interest

There are no conflicts to declare.

Acknowledgements

The authors thank the nanofabrication facility in ZJUI and micro/nanofabrication in USTC. This work was led by Prof. Huan Hu and Prof. Oleksiy Penkov. The work was funded by NSFC normal grant (Grant No. 61974128), the Natural Science Foundation of Zhejiang Province (Grant No. LY19F040007), the Center of Pathogen Detection in the Dynamic Research Enterprise for Multidisciplinary Engineering Sciences (DREMES), Cyrus Tang Foundation, and the Technical Promotion Plan of USTC (No. TS2021006).

Notes and references

1 J. M. Mativetsky, Y.-L. Loo and P. Samorì, *J. Mater. Chem. C*, 2014, **2**, 3118–3128.
2 L. Sun, Y. A. Diaz-Fernandez, T. A. Gschneidtner, F. Westerlund, S. Lara-Avila and K. Moth-Poulsen, *Chem. Soc. Rev.*, 2014, **43**, 7378–7411.
3 M. Liao, P. Nicolini, L. Du, J. Yuan, S. Wang, H. Yu, J. Tang, P. Cheng, K. Watanabe, T. Taniguchi, L. Gu, V. E. P. Claerbout, A. Silva, D. Kramer, T. Polcar, R. Yang, D. Shi and G. Zhang, *Nat. Mater.*, 2022, **21**, 47–53.
4 O. Werzer, E. D. Cranston, G. G. Warr, R. Atkin and M. W. Rutland, *Phys. Chem. Chem. Phys.*, 2012, **14**, 5147–5152.

Published on 13 September 2022. Downloaded by Zhejiang University on 2/23/2024 3:47:54 AM.

5 O. Guillaume-Gentil, C. G. Gäbelein, S. Schmieder, V. Martinez, T. Zambelli, M. Künzler and J. A. Vorholt, *Commun. Biol.*, 2022, **5**, 180.
6 M. Reggente, D. Passeri, L. Angeloni, F. A. Scaramuzzo, M. Barteri, F. De Angelis, I. Persiconi, M. E. De Stefano and M. Rossi, *Nanoscale*, 2017, **9**, 5671–5676.
7 L. G. Rosa and J. Liang, *J. Phys.: Condens. Matter*, 2009, **21**, 483001.
8 S. Handschuh-Wang, T. Wang and X. Zhou, *RSC Adv.*, 2017, **7**, 47464–47499.
9 S. Benaglia, C. A. Amo and R. Garcia, *Nanoscale*, 2019, **11**, 15289–15297.
10 G. Gururajan, S. P. Sullivan, T. P. Beebe, D. B. Chase and J. F. Rabolt, *Nanoscale*, 2011, **3**, 3300–3308.
11 J. O. de Beeck, N. Labyedh, A. Sepulveda, V. Spampinato, A. Franquet, T. Conard, P. M. Vereecken and U. Celano, *Nanoscale*, 2018, **10**, 12564–12572.
12 K. Panda, J.-E. Kim, K. J. Sankaran, I. N. Lin, K. Haenen, G. S. Duesberg and J. Y. Park, *Nanoscale*, 2021, **13**, 7308–7321.
13 T. Strahlendorff, G. Dai, D. Bergmann and R. Tutsch, *Ultramicroscopy*, 2019, **201**, 28–37.
14 W. A. Ducker, T. J. Senden and R. M. Pashley, *Nature*, 1991, **353**, 239–241.
15 B. Babel and M. Rudolph, *MethodsX*, 2019, **6**, 651–659.
16 P. M. Young, M. J. Tobyn, R. Price, M. Buttrum and F. Dey, *J. Pharm. Sci.*, 2006, **95**, 1800–1809.
17 X. N. Xie, H. J. Chung, C. H. Sow and A. T. S. Wee, *Mater. Sci. Eng., R*, 2006, **54**, 1–48.
18 R. Garcia, A. W. Knoll and E. Riedo, *Nat. Nanotechnol.*, 2014, **9**, 577–587.
19 N. Orji, R. Dixson, E. Lopez and B. Irmer, *J. Micro/Nanolithogr., MEMS, MOEMS*, 2020, **19**, 014004.
20 K.-H. Chung, *Int. J. Precis. Eng. Manuf.*, 2014, **15**, 2219–2230.
21 B. A. Gozen and O. B. Ozdoganlar, *Wear*, 2014, **317**, 39–55.
22 P. M. Claesson, I. Dobryden, G. Li, Y. He, H. Huang, P.-A. Thorén and D. B. Haviland, *Phys. Chem. Chem. Phys.*, 2017, **19**, 23642–23657.
23 K. E. Petersen, *Proc. IEEE*, 1982, **70**, 420–457.
24 R. Maboudian, *Surf. Sci. Rep.*, 1998, **30**, 207–269.
25 C. Ventosa, F. Rieutord, L. Libralesso, C. Morales, F. Fournel and H. Moriceau, *J. Appl. Phys.*, 2008, **104**, 123524.
26 E. Taran, B. C. Donose, I. U. Vakarelski and K. Higashitani, *J. Colloid Interface Sci.*, 2006, **297**, 199–203.
27 C. H. Scholz, *Nature*, 1998, **391**, 37–42.
28 Q. Li, T. E. Tullis, D. Goldsby and R. W. Carpick, *Nature*, 2011, **480**, 233–236.
29 A. Li, Y. Liu and I. Szlufarska, *Tribol. Lett.*, 2014, **56**, 481–490.
30 J. Yeon, A. C. T. van Duin and S. H. Kim, *Langmuir*, 2016, **32**, 1018–1026.
31 L. Bocquet, E. Charlaix, S. Ciliberto and J. Crassous, *Nature*, 1998, **396**, 735–737.
32 L. Chen, H. He, X. Wang, S. H. Kim and L. Qian, *Langmuir*, 2015, **31**, 149–156.
33 H. Hu, B. Shi, C. M. Breslin, L. Gignac and Y. Peng, *Langmuir*, 2020, **36**, 7861–7867.
34 E. Rabinowicz, *Friction and Wear of Materials*, Wiley-Interscience; New York, 2nd edn, 1995.
35 L. M. Leidens, M. E. H. Maia da Costa, N. S. Figueroa, R. A. Barbieri, F. Alvarez, A. F. Michels and C. A. Figueroa, *Phys. Chem. Chem. Phys.*, 2021, **23**, 2873–2884.
36 H. J. Butt and M. Jaschke, *Nanotechnology*, 1995, **6**, 1–7.
37 H. Sadeghian, J. F. L. Goosen, A. Bossche, B. J. Thijsse and F. van Keulen, *Thin Solid Films*, 2011, **520**, 391–399.
38 X. Li, T. Ono, Y. Wang and M. Esashi, *Appl. Phys. Lett.*, 2003, **83**, 3081–3083.
39 S. H. Park, J. S. Kim, J. H. Park, J. S. Lee, Y. K. Choi and O. M. Kwon, *Thin Solid Films*, 2005, **492**, 285–289.
40 R. E. Miller and V. B. Shenoy, *Nanotechnology*, 2000, **11**, 139–147.
41 H. Sadeghian, C.-K. Yang, J. F. L. Goosen, A. Bossche, U. Staufer, P. J. French and F. van Keulen, *J. Micromech. Microeng.*, 2010, **20**, 064012.
42 B. K. Gupta and B. Bhushan, *Surf. Coat. Technol.*, 1994, **68-69**, 564–570.
43 Z. De-kun, G. Shi-rong and W. Qing-liang, *Tribol. Int.*, 2009, **42**, 1399–1404.
44 E. V. Jelenkovic, S. To, L. V. Goncharova and S. F. Wong, *Mater. Res. Express*, 2017, **4**, 075013.
45 B.-K. Jang, *J. Alloys Compd.*, 2006, **426**, 312–315.
46 P. Herre, S. Romeis, M. Mačković, T. Przybilla, J. Paul, J. Schwenger, B. Torun, G. Grundmeier, E. Spiecker and W. Peukert, *J. Am. Ceram. Soc.*, 2017, **100**, 5709–5722.
47 H. Jami and A. Jabbarzadeh, *Appl. Surf. Sci.*, 2019, **489**, 446–461.
48 L. Yang, J. J. Bian, H. Zhang, X. R. Niu and G. F. Wang, *AIP Adv.*, 2015, **5**, 077162.
49 J. Yin, M. Retsch, J.-H. Lee, E. L. Thomas and M. C. Boyce, *Langmuir*, 2011, **27**, 10492–10500.
50 P. C. Fletcher, J. R. Felts, Z. Dai, T. D. Jacobs, H. Zeng, W. Lee, P. E. Sheehan, J. A. Carlisle, R. W. Carpick and W. P. King, *ACS Nano*, 2010, **4**, 3338–3344.
51 B. V. Derjaguin, V. M. Muller and Y. P. Toporov, *J. Colloid Interface Sci.*, 1975, **53**, 314–326.
52 B. Gotsmann and M. A. Lantz, *Phys. Rev. Lett.*, 2008, **101**, 125501.
53 J. Liu, D. S. Grierson, N. Moldovan, J. Notbohm, S. Li, P. Jaroenapibal, S. D. O'Connor, A. V. Sumant, N. Neelakantan, J. A. Carlisle, K. T. Turner and R. W. Carpick, *Small*, 2010, **6**, 1140–1149.
54 J. S. Villarrubia, *J. Res. Natl. Inst. Stand. Technol.*, 1997, **102**, 425–454.
55 X. Wen, R. Mao and H. Hu, *Adv. Mater. Interfaces*, 2022, **9**, 2101643.
56 J. Chen, I. Ratera, J. Y. Park and M. Salmeron, *Phys. Rev. Lett.*, 2006, **96**, 236102.
57 L. T. Zhuravlev, *Colloids Surf., A*, 2000, **173**, 1–38.
58 G. Vigil, Z. Xu, S. Steinberg and J. Israelachvili, *J. Colloid Interface Sci.*, 1994, **165**, 367–385.
59 E. Riedo, F. Lévy and H. Brune, *Phys. Rev. Lett.*, 2002, **88**, 185505.
60 R. Szoszkiewicz and E. Riedo, *Phys. Rev. Lett.*, 2005, **95**, 135502.

 This journal is © the Owner Societies 2022

61 J. J. Adler, Y. I. Rabinovich and B. M. Moudgil, *J. Colloid Interface Sci.*, 2001, **237**, 249–258.
62 J.-H. Horng, M.-L. Len and J.-S. Lee, *Wear*, 2002, **253**, 899–913.
63 N. S. Tambe and B. Bhushan, *Nanotechnology*, 2005, **16**, 2309–2324.
64 L. Chen, S. H. Kim, X. Wang and L. Qian, *Friction*, 2013, **1**, 81–91.
65 S. Lafaye, C. Gauthier and R. J. T. L. Schirrer, *Tribol. Lett.*, 2006, **21**, 95–99.
66 M. K. Beyer, *J. Chem. Phys.*, 2000, **112**, 7307–7312.
67 Z. Zhang, S. Pan, N. Yin, B. Shen and J. Song, *Friction*, 2021, **9**, 119–131.
68 A. L. Barnette, D. B. Asay, D. Kim, B. D. Guyer, H. Lim, M. J. Janik and S. H. Kim, *Langmuir*, 2009, **25**, 13052–13061.

Published on 13 September 2022. Downloaded by Zhejiang University on 2/23/2024 3:47:54 AM.